Investigations of fast neutron production by 190 GeV/c muon interactions on graphite target

V. Chazal [a,*], F. Boehm [b], B. Cook [b,1], H. Henrikson [b], G. Jonkmans [a], A. Paic [a,2], N. Mascarenhas [b,3], P. Vogel [b], J.-L. Vuilleumier [a]

[a] *Institut de Physique, Université de Neuchâtel, 2000 Neuchâtel, Switzerland*

[b] *California Institute of Technology, Pasadena CA 91125, U.S.A.*

Abstract

The production of fast neutrons (1 MeV - 1 GeV) in high energy muon-nucleus interactions is poorly understood, yet it is fundamental to the understanding of the background in many underground experiments. The aim of the present experiment (CERN NA55) was to measure spallation neutrons produced by 190 GeV/c muons scattering on carbon target. We have investigated the energy spectrum and angular distribution of spallation neutrons, and we report the result of our measurement of the neutron production differential cross section.

Key words: underground neutron flux, fast neutron production, muon-nucleus interaction, time-of-flight
PACS: 25.30.Mr, 25.20.-x, 25.40.Sc, 28.20.-v

1 Introduction

Neutrons are an important source of background in many low rate underground experiments. Detectors such as the Palo Verde detector [1], the Kamiokande detector [2], the Edelweiss detector [3], the Stanford Underground

* corresponding author.
Email address: verene.chazal@unine.ch (V. Chazal).
1 Present address: Jet Propulsion Laboratory, Pasadena CA 91109, U.S.A.
2 Present address: Monitor Company, 12 Place Vendôme, 75001 Paris, France
3 Present address: Foveon Inc., 3565 Monroe St., Santa Clara CA 95051, U.S.A.

Facility detector [4], the Gallex detector [5], and most of the other underground experiments are concerned with neutron background. It is therefore important to understand the different neutron production mechanisms in the environment of such experiments.

There are two sources of neutrons in underground laboratories. The first one is the natural radioactivity such as (α,n) reactions and spontaneous fission, due to uranium and thorium traces in the rock or in the materials used in the experiments themselves. The second source is the interaction of atmospheric muons, produced by cosmic rays, with matter, such as the surrounding rock, the different shieldings or the detector itself. Propagating through matter, muons lose energy mainly continuously by ionization. In addition, they lose energy in discrete bursts along their trajectory by bremsstrahlung, direct pair production and nuclear interactions [6]. The goal of the present experiment (CERN NA55) was to study neutron production in muon-nucleus interactions, which at present is poorly understood. In this paper we report the result of our measurement of the cross section for fast neutron production by interaction of high energy muons off carbon nuclei. Specifically, we investigated the energy spectrum and angular distribution of spallation neutrons produced by the inelastic scattering of 190 GeV/c muons on a graphite target, via the time-of-flight method. Data has also been obtained for copper, lead and concrete targets and the results of a forthcoming analysis will be published later.

2 Interaction of high energy muons with matter

The total neutron yield measured at different depths has been reported in references [1] and [7]. However, very little is known about the energy and angular distributions of the neutrons. Moreover, one expects that many neutrons are produced in secondary processes following the primary muon-nucleus interaction and it is difficult to separate the two effects in the inclusive measurements performed underground.

To describe the process theoretically, one assumes that the muon scattering occurs primarily at very small angles. Such a process can be viewed as produced by a beam of nearly real equivalent photons [8]. Even with this drastic simplification, it is difficult to obtain reliable estimates for actual yields and spectra of the neutrons. The difficulty lies in the estimation of the equivalent photon flux, as well as in the shortage of experimental nuclear photo-disintegration data for high energy photons.

3 Experimental apparatus

3.1 Experimental set-up

The layout of our NA55 experiment is similar to a CERN LEAR experiment [9] in which neutrons and pions were measured following anti-protons stopping in the target. Another group, E665 at Fermi-lab [10], measured neutrons produced by deep-inelastic scattering of 470 GeV/c muons. However, the latter experiment measured neutrons in a small energy range from 1 to 10 MeV, with high-energy deep inelastically scattered muons from nuclear targets. In the frame of the CERN NA54 experiment, measurements were done on a carbon target to study the production of radioactive isotopes in scintillation detectors by 100 and 190 GeV muons and their secondary shower particles [11].
The M2 muon beam at the CERN-SPS was well suited for our investigation. At 190 GeV/c, the energy of the SPS muons is similar to the mean energy of cosmic-ray muons at many underground experimental sites. The beam transverse size is 2.2 cm (FMWH). Our experiment was performed with a cylindrical graphite target of 75 cm length and 8 cm diameter. Three neutron detectors (see section 3.2) were placed at 45 (N1), 90 (N2) and 135 (N3) degrees relative to the muon beam, for a target-detector distance of 2.20 m (see Fig. 1). A beam counter H6 (from NA47 experiment [12]) consisting of plastic scintillators is placed directly in the muon beam and is thus exposed to rates of about 20 MHz, during the two-seconds beam-on phase. To reduce the detector rate to a manageable level, the target is segmented into 4 rings, each divided in 16 counters thus reducing the rate per phototube to at most 1 MHz in the center. Several large plastic scintillators are placed upstream from the neutron detectors and are used to veto muons originating from the beam halo. An iron hadron absorber was placed far behind the target along the beam axis.

3.2 The neutron detectors and electronics

Each detector is a 20 x 20 cm cylindrical glass vessel, equiped with two photomultipliers (Philips XP4512 photomultipliers with fast 1.1 nsec RMS pulse) and filled with Bicron 501A liquid scintillator which possesses excellent pulse shape discrimination properties for neutron identification [13]. Thin plastic scintillators (7 mm) are positioned in front of and around each neutron detector to tag charged particles, such as protons and pions. They are also used to veto the cosmic muons.
The particle energy is measured via the time-of-flight (TOF) from its production site in the target. The signal of the neutron detector provides the TOF start, and the signal of the segmented beam counter, located 6 m upstream

from the target, is delayed to provide the TOF stop. The analog signals of each of the neutron counters N were coded using 3 different CAMAC ADC's digitizing respectively the full analog pulse, the pulse rise and the pulse tail. The pulse itself provided the three ADC gates by means of a low-threshold discriminator, which also provides a CAMAC multi-hit TDC with the TOF start signal. The analog signals of each of the plastic scintillators S were coded using 15 different CAMAC ADC's.

4 Neutron detector efficiency

The neutron detection efficiency was simulated using the GCALOR Monte Carlo package [14]. Neutrons were generated with energies from 2 to 1000 MeV. The efficiency for neutrons entering the detector was obtained as a function of both the detector energy threshold and the neutron energy. The geometrical acceptance of the detector, the quenching effect and each detector threshold were taken into account. The calculation of scintillator quenching was taken from Ref. [15], as the amount of light depends on the particle type and is not directly proportional to the deposited energy. Above a neutron energy of 50 MeV, the electron equivalent energy in the scintillator is assumed to be a linear function of the proton energy [16], with a proportionality constant of 0.83. Below 50 MeV, we applied the following formula:

$$T_e \ = \ 0.83 \ T_p \ - \ 2.82 \ \left[\ 1.0 - e^{\left(\ - \ 0.25 \ T_p^{0.93} \right)} \right] \tag{1}$$

where T_e was the electron energy in MeV and T_p the proton energy in MeV. As will be shown later, the neutron energy spectrum in each counter is peaked at lower energies. Therefore, the detection efficiency is strongly dependent upon the neutron detectors thresholds. The thresholds are determined from the energy loss spectrum of cosmic muons in the Bicron cells. Vertical muons (cosmics) are selected by requiring a coincidence signal above pedestals in the top and bottom scintillation counters during beam-off runs. Because of the hardware thresholds, these spectra show a clear cut-off at low energy. The neutron detector thresholds are then extracted by a comparison with a simulated energy spectrum of cosmic muons with the measured one. The Monte Carlo spectrum of cosmic muons $N(E)$ is then convoluted with a gaussian response function, $R(E, H)$ for the detectors:

$$N(H) = \int_0^E R(H, E) N(E) dE \tag{2}$$

where $N(H)$ is the measured spectrum in ADC counts H. The response function parameters are of the same form as the ones used by Arneodo *et al.* [13] who have described and tested the response of similar Bicron 501A liquid scintillator cells. Applying this procedure, we obtain thresholds of 4.8 ± 0.4 MeV for N1, 5.5 ± 0.3 MeV for N2 and 6.9 ± 0.3 MeV for N3.

Finally, Fig. 2 shows the Monte Carlo simulation of the neutron detection efficiency as a function of both neutron energy and energy threshold. Neutrons were assumed to be detected only if recoil protons ionize heavily and stop in the scintillator producing delayed light and thus making pulse shape discrimination possible.

5 Data analysis

The experiment was performed from April to June 1996. The results of the analysis of our data from the graphite target is presented bellow.

5.1 Background

The challenge of this experiment is to discriminate neutrons from the abundant bremsstrahlung photons. Furthermore, four other background sources may contribute to the measured spectra: charged particles from the target, cosmic muons, muons from the beam and ambient neutrons. Cosmic muons and charged particles can be rejected using the plastic scintillators. Muons from the beam halo are eliminated by the dedicated veto counter (HV, see Fig. 1). Surrounding neutrons cannot be eliminated, but their contribution can be estimated from dedicated empty-target runs. Finally, neutrons and photons are identified by a pulse shape discrimination (PSD) of their signal in the liquid scintillator.

5.2 Pulse shape discrimination

The time-development of scintillation light depends on the nature of the ionising particle. Measuring the signal at 2 different time intervals allows to build a PSD plot [17]. The complete PSD method is explained in Ref. [18]. Fig. 3 shows the signal obtained in a delayed window as a function of the signal measured in a prompt one (PSD1). Based on the same principle, Fig. 4 is obtained with other intervals in the pulse (PSD2). In these two different PSD representations, we can distinguish a γ-like curve containing bremsstrahlung photons and cosmic and remaining beam halo muons, and a neutron-like zone containing all the neutrons and the charged hadrons from the target. The γ-like events are easily selected from the time-of-flight since they are prompt with respect to the beam muons. Then we calculate the real distance (in units of channel number) between every points and the fitted γ-like curve for the PSD1 (distance 1) and the PSD2 (distance 2). We can then represent distance 1 as a function of distance 2, for all events including the charged particles. Figure 5 shows the events left after the cuts which selects only neutral particles. A clear separation can be seen between photons and neutrons. The cut efficiency is computed from the (n,γ) discrimination, applying a gaussian fit on the neutron and gamma peaks. A 2σ cut on the neutron peak leads to the eliminated neutron rate and the excess gamma rate. The global cut efficiency is 85.5%, 66.5% and 61.9% for the N1, N2 and N3 detectors respectively. These discriminated neutron events can then be selected for the time-of-flight analysis.

5.3 Time-of-flight analysis

Before being converted into energy distributions, the selected neutron time-of-flight spectra must be corrected for off-target events and for random TOF stop signals. The first background arises from triggers correlated with beam particles, as neutrons bouncing on the ground or walls, for example. Their contribution can be deduced from 'empty target' runs properly normalized to the incident flux. The second background component is due to multiple TOF stop signals given by randomly incoming muons hitting the H6 detector scintillators. As their time distribution is flat (see Fig. 6), they can be easily subtracted.

The calibration of the time spectrum is obtained from the gamma peak, with a time resolution of 1.0 ns, 4.6 ns and 3.8 ns for N1, N2 and N3 respectively. As a consequence, we measure maximum neutron energy of around 1 GeV, 250 MeV and 310 MeV for N1, N2 and N3 respectively. The energy distribution is computed from the TOF distribution, and corrected for the detector efficiency as described in section 4.

6 Results

6.1 Additional acceptance corrections

The charged particle rejection using the scintillators S leads to a loss of good neutron events. The corresponding acceptances are determined from the comparison of neutron samples with and without scintillator cut for each neutron detectors, and strongly depend on the scintillator efficiencies and thresholds. The acceptances are (66.9±0.1)%, (82.3±0.1)%, (66.3±0.1)% for N1, N2 and N3 respectively. In addition, the 85 Hz trigger rate for all detectors above a threshold of 50 MeV leads to a dead time of 2.1%. All the efficiencies taken into account in the calculation of the neutron production cross section are summarized in Table 1.

6.2 Production cross section and energy spectrum

The neutron production cross section was calculated using the following formula:

$$\frac{d\sigma}{d\Omega}(\Theta \pm \Delta\Theta) = \left(\frac{dn}{\phi\ N\ d\Omega}\right) \tag{3}$$

where dn is the number of selected neutrons corrected for all acceptances. All parameters are given in Table 2. Figure 7 shows the differential neutron production cross section as a function of the neutron energy, including all efficiencies corrections, for the three different angles. The energy integrated values from the corresponding threshold up, are gathered in Table 3. It is worth noting that the neutron energy spectrum is displaced towards low energies when going from forward to backward angles. As a consequence, no neutrons are detected above 70 MeV at 135°. Our angular and energy distributions agree with the FLUKA simulation performed by Wang *et al.* [19]. Our measurements show that the angular distribution is forward peaked, with the exception of the lowest energy bin. This effect can be understood as due to the motion of the source nucleus combined with an isotropic distribution of the emitted neutron at the lowest energies.

7 Conclusion

We investigated the production of spallation neutrons obtained from 190 GeV/c muons scattering on a graphite target. The neutrons were observed by liquid scintillator detectors, allowing background rejection by means of pulse shape discrimination. The neutron energy distribution was determined via time-of-flight. The 190 GeV muon energy corresponds to the mean energy of cosmic-ray muons at underground experimental sites of about 2000 meters water equivalent depth. However, in the present experiment only neutrons associated with the primary muon-nuclear spallation process are detected, while in the underground detectors the total neutron yields are measured. Thus the present experiment is not dependent on the subsequent neutron transport and multiplication. In view of this, and also in the view of the difference in the muon spectrum (narrow vs. broad distribution) direct comparison is difficult. Nevertheless, the cross sections quoted in Table 3 are in a qualitative agreement with the yields underground and, as mentioned above, their shape agrees with the FLUKA simulation.
Results on neutron angular distribution and energy distribution were obtained for the first time. The differential cross section as a function of the neutron energy were obtained for 45°, 90° and 135° production angles with around 15% accuracy. Data has also been recorded for copper, lead and concrete targets and their analysis will be presented in a forthcoming paper.

Acknowledgements

Special thanks go to G. Gervasio for his contribution to the data decoding and O. Drapier for many useful discussions. We are grateful to D. Hilscher of HMI, Berlin for providing us with a PSD module. We thank H. Wong, A. Schopper, L. Gatignon and the staff at CERN for assistance provided. The PSI, Villigen for help with calibrating our neutron detectors is also acknowledged. This project was supported in part by the US Department of Energy.

References

[1] F. Boehm *et al.,* Phys. Rev. D62 (2000) 092005.

[2] Y. Fukuda *et al.,* Phys. Lett. B388 (1996) 397.

[3] V. Chazal *et al.,* Astropart. Phys. 9 (1998) 163.

[4] A. Da Silva *et al.,* Nucl. Instrum. Meth. A354 (1995) 553.
S.R. Golwala *et al.,* Nucl. Instrum. Meth. A444 (2000) 345.

[5] M. Cribier *et al.,* Astropart. Phys. 4 (1995) 23.

[6] T.K. Gaisser, Cosmic Rays and Particle Physics, Cambridge University Press (1990).

[7] R. Hertenberger *et al.,* Phys. Rev. C52 (1995) 3449.
L.B. Bezrukov *et al.,* Sov. J. Nucl. Phys. 17 (1973) 51.
R.I. Enikeev *et al.,* Sov. J. Nucl. Phys. 46 (1987) 883.
M. Aglietta *et al.,* hep-ex/9905047.
M. Aglietta *et al.,* Nuovo Cim. C12 (1989) 467.

[8] J. Delorme *et al.,* Phys. Rev. C52 (1995) 2222.

[9] D. Polster *et al.,* Phys. Rev. C51 (1995) 1167.

[10] M.R. Adams *et al.,* Phys. Rev. Lett. 74 (1995) 5198. Erratum-ibid. 80 (1998) 2020.

[11] T. Hagner *et al.,* Astropart. Phys. 14 (2000) 33.

[12] SMC (NA47) Collaboration, SPSC/88-47/P242.

[13] F. Arneodo *et al.,* Nucl. Instrum. Meth. A418 (1998) 285.

[14] C. Zeitnitz and T.A. Gabriel, Nucl. Instrum. Meth. A349 (1994) 106.

[15] R.A. Cecil *et al.,* Nucl. Instrum. Meth. 161 (1979) 439.

[16] R.L. Craun and D.L. Smith, Nucl. Instrum. Meth. 80 (1970) 239.
Y. Uwamino *et al.,* Nucl. Instrum. Meth. 204 (1982) 179.

[17] F.D. Brooks, Nucl. Instrum. Meth. 4 (1959) 151.
G. Ranucci, Nucl. Instrum. Meth. A354 (1995) 389.

[18] G.F. Knoll, Radiation Detection and Measurement; 3rd ed, John Wiley (2000).

[19] Y-F. Wang *et al.,* hep-ex/0101049.

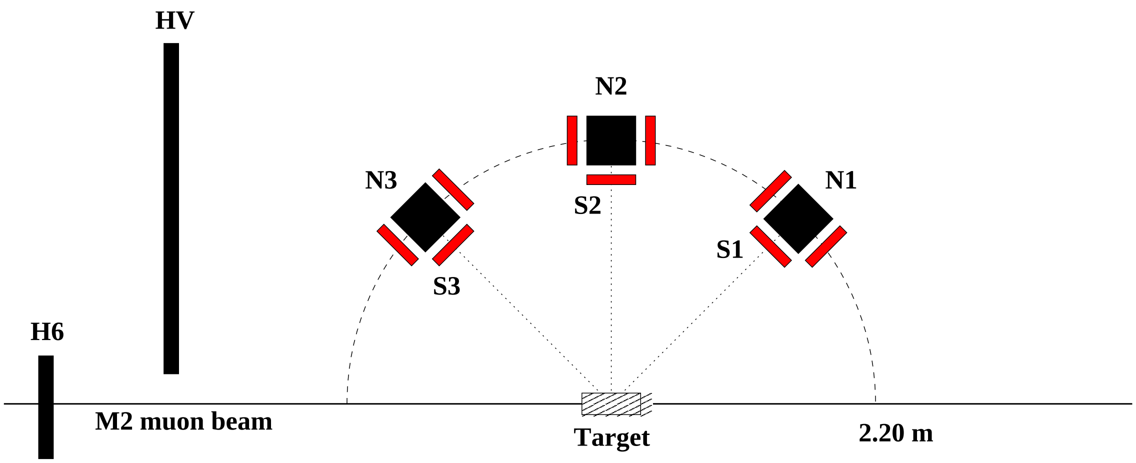

Fig. 1. NA55 detector layout. N: Bicron 501A liquid scintillator detectors with Pulse Shape Discrimination. S: thin plastic scintillator counters for charged particle identification, in front and around each N detector. H6: NA47 segmented high rate beam counter. HV: beam muon halo veto, thin plastic scintillator. Arbitrary figure scale.

Table 1
Acceptance of analysis cuts

Analysis cuts	N1 (45°)	N2 (90°)	N3 (135°)
PSD cuts	85.5%	66.5%	61.9%
Plastic scintillators	(66.9 ± 0.1)%	(82.3 ± 0.1)%	(66.3 ± 0.1)%
Dead time		97.9%	

Table 2
Summary of calculated cross-section parameters

parameter	value	
Muon beam flux ϕ	1.63 x 10^{11} muons	
Graphite target density N=ρL	(8.52 ± 0.11) x 10^{24} atoms/cm^2	
Angular acceptance $d\Omega$	(5.2 ± 0.6) x 10^{-4} sr	
Energy spectrum integral corrected	45°	103900 neutrons
for the corresponding	90°	52050 neutrons
detector efficiency	135°	28900 neutrons

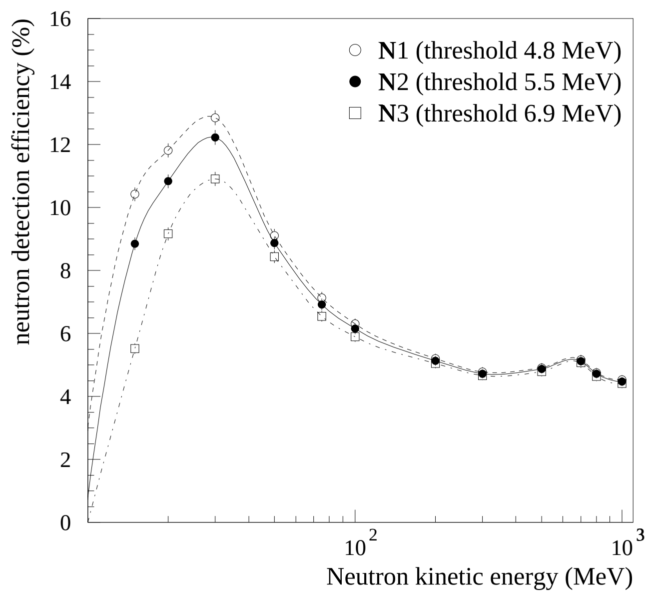

Fig. 2. Simulation of the neutron detection efficiency as a function of neutron energy and threshold, taking into account the geometrical acceptance of the detector and the quenching effect, for the angles 45° (N1), 90° (N2) and 135° (N3). A polynomial interpolations (dotted, solid and dashed lines) have been obtained from the simulated efficiencies (open circles, solid circles and open squares) and used for the efficiency corrections. The bump at 700 MeV is the result of an approximation.

Table 3
Differential neutron production cross-section

Differential cross section	barn/sr	neut/μ.g.sr.cm^{-2}
$\frac{d\sigma}{d\Omega}(45° \pm 1°)$	(2.18 ± 0.31) x 10^{-4}	(1.09 ± 0.16) x 10^{-5}
$\frac{d\sigma}{d\Omega}(90° \pm 1°)$	(8.86 ± 1.25) x 10^{-5}	(0.45 ± 0.06) x 10^{-5}
$\frac{d\sigma}{d\Omega}(135° \pm 1°)$	(6.11 ± 0.90) x 10^{-5}	(0.31 ± 0.05) x 10^{-5}

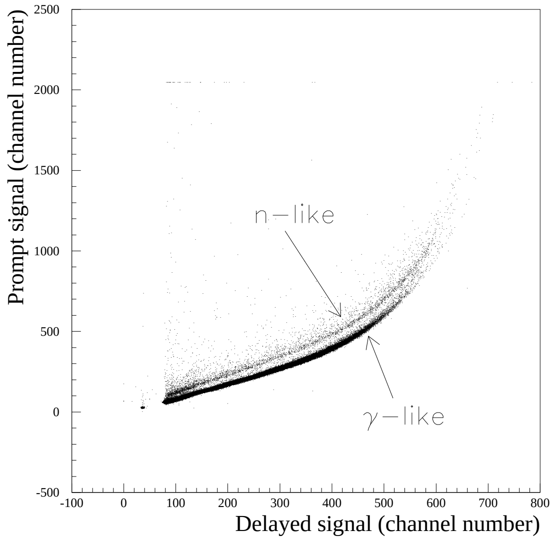

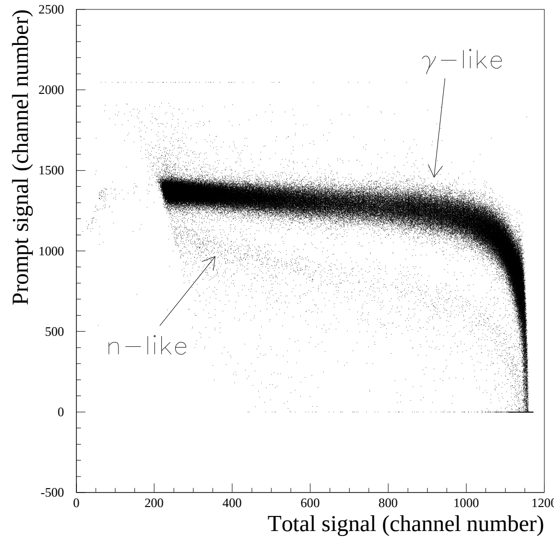

Fig. 3. First pulse shape discrimination (PSD1) for the N1 detector. The signal is measured into 2 different time intervals : prompt signal amplitude vs. delayed signal amplitude.

Fig. 4. Second pulse shape discrimination (PSD2) for the N1 detector. Prompt signal amplitude vs. total signal amplitude.

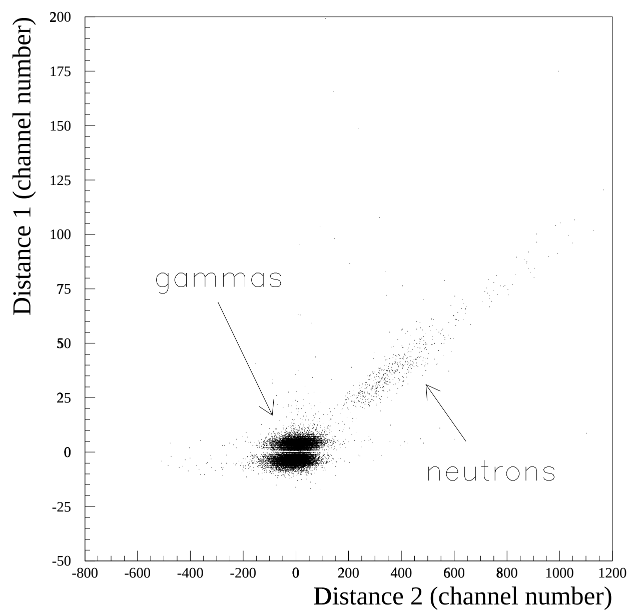

Fig. 5. Distance 1 vs. distance 2 for the N1 detector. These distances were calculated between every point and the γ-like events for PSD1 and PSD2. Only neutral particles are selected.

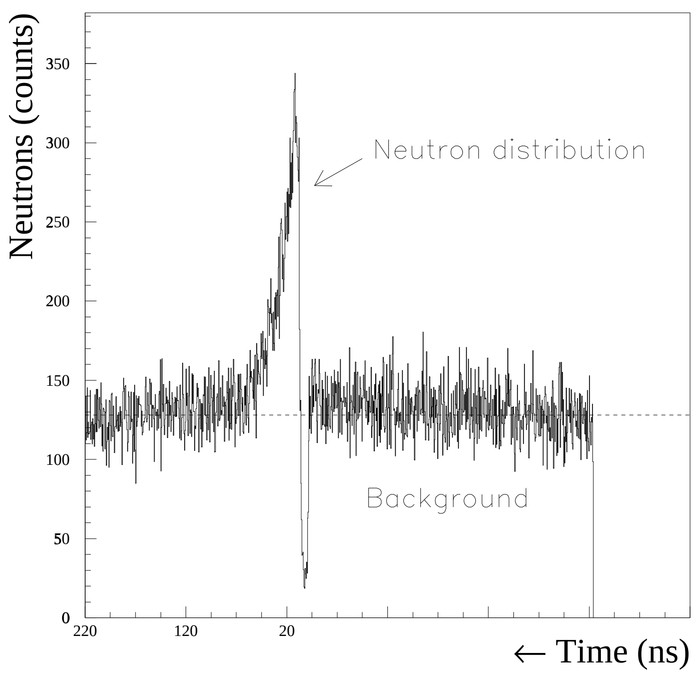

Fig. 6. TDC spectrum corresponding to the neutron distribution dn/dt. The undershoot for times immediately before the 'prompt' signal is caused by the removal of the gamma peak. The background due to uncorrelated beam muons is flat.

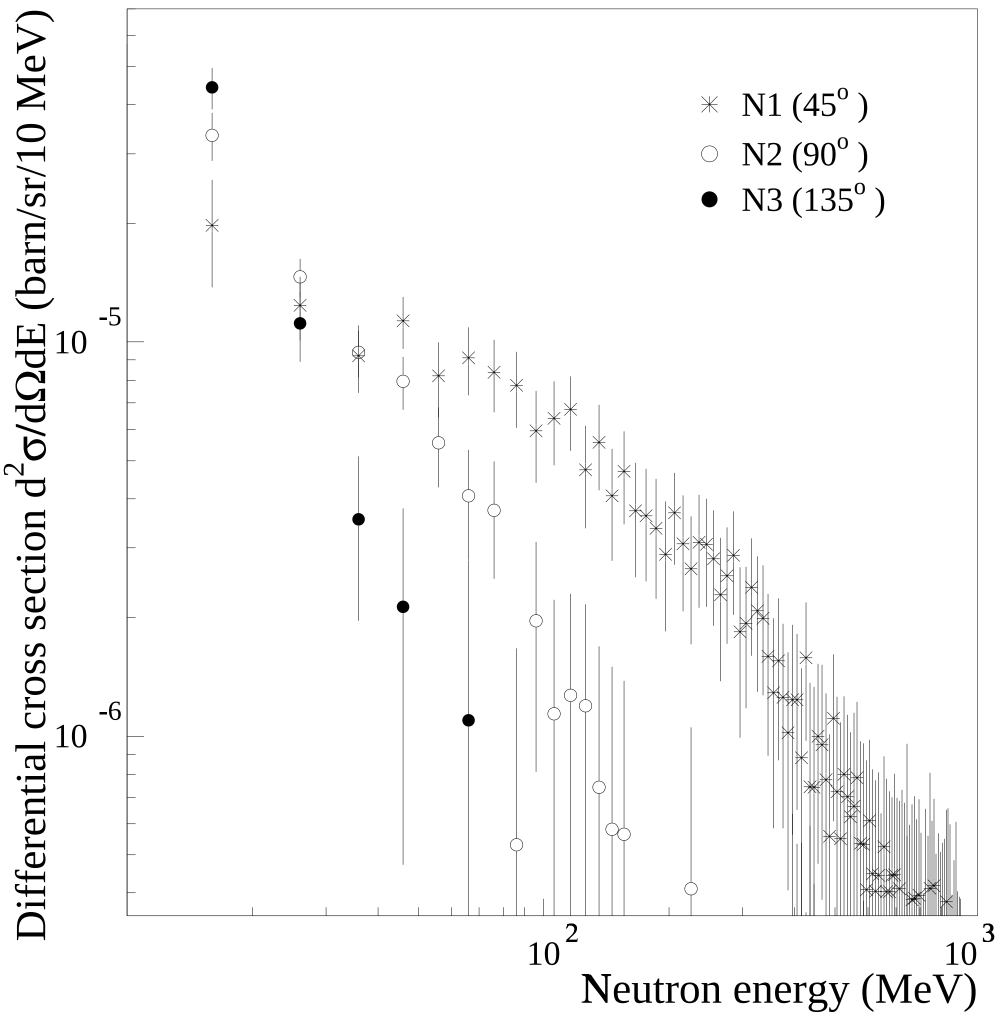

Fig. 7. Neutron energy spectrum, including all the corrections.